Journal of Nanostructure in Chemistry (2022) 12:963–977
https://doi.org/10.1007/s40097-021-00466-x

ORIGINAL RESEARCH

Towards investigating the characteristics and thermal kinetic behavior of emergent nanostructured nitrocellulose prepared using various sulfonitric media

Ahmed Fouzi Tarchoun[1,2] · Zakaria Bekkar Djelloul Sayah[3] · Djalal Trache[1] · Thomas M. Klapötke[4] · Mekki Belmerabt[1] · Amir Abdelaziz[1] · Slimane Bekhouche[1]

Received: 11 September 2021 / Accepted: 7 December 2021 / Published online: 18 January 2022

Abstract

With the aim of developing promising generation of cellulose-based energetic materials, nanostructured nitrocellulose biopolymers (NNCs) were prepared from cellulose microcrystals using different sulfonitric media. Their molecular structure, physicochemical features, crystallinity and thermal behavior were examined to scrutinize the nitration processes by pointing out the effect of nitric acid content in the nitrating medium. The experimental findings showed that the produced NNCs displayed outstanding properties, including elevated density (≥ 1.689) and great substitution degree (≥ 2.58), which are higher than those of the conventionally used pristine nitrocellulose (NC). Furthermore, it was found that the increase of nitric acid concentration from 70 to 100% promoted the nitrogen content, density and viscosity-average molecular weight of the as-prepared NNCs, whereas, their crystallinity index and thermal stability decreased. Their non-isothermal decomposition kinetics were also investigated using isoconversional approaches, revealing a decreased trend of the Arrhenius parameters from NNC-70 to NNC-100, and hence following different decomposition models. Consequently, these results enrich future prospects for the design of new generation of energetic nanostructured cellulosic biopolymers for potential use in advanced composite explosives and solid propellants.

Keywords Nitrocellulose · Cellulose microcrystals · Nitration · Physicochemical properties · Kinetic analysis

Introduction

In the field of energy-rich biopolymers, nitrated cellulose, commonly known as nitrocellulose (NC), remains the most popular and extensively used cellulose-based energetic derivatives in several civilian and military applications, owing to its intriguing and unique characteristics [1–4]. This fluffy white carbohydrate biopolymer is typically produced by a reversible and highly exothermic esterification of ordinary cellulose derived from a wide range of natural sources for which wood pulp and cotton linters are the most often utilized feedstocks [5, 6]. The hierarchical structure of NC is basically composed of D-glucopyranosyl units linked by chemical β-glycosidic bonds between the C1 of one pyranose ring and the C4 of the next ring to produce the basic elementary fibrils [7, 8]. Each repetitive unit possesses three carbons, which are encountered with nitrate esters ($O–NO_2$) groups formed by the electrophilic substitution of hydronium ions (H^+) of hydroxyl groups (OH) with the nitronium ones (NO_2^+), as illustrated in Scheme 1. In this context, several

✉ Ahmed Fouzi Tarchoun
tarchounfouzi@gmail.com

✉ Djalal Trache
djalaltrache@gmail.com

1 Energetic Materials Laboratory, Teaching and Research Unit of Energetic Processes, Ecole Militaire Polytechnique, Bordj El-Bahri, BP 17, 16046 Algiers, Algeria

2 Energetic Propulsion Laboratory, Teaching and Research Unit of Energetic Processes, Ecole Militaire Polytechnique, Bordj El-Bahri, BP 17, 16046 Algiers, Algeria

3 Macromolecular Chemistry Laboratory, Teaching and Research Unit of Physical Chemistry Materials, Ecole Militaire Polytechnique, Bordj El-Bahri, BP 17, 16046 Algiers, Algeria

4 Department of Chemistry, Ludwig Maximilian University, Butenandtstrasse 5-13 (D), 81377 Munich, Germany

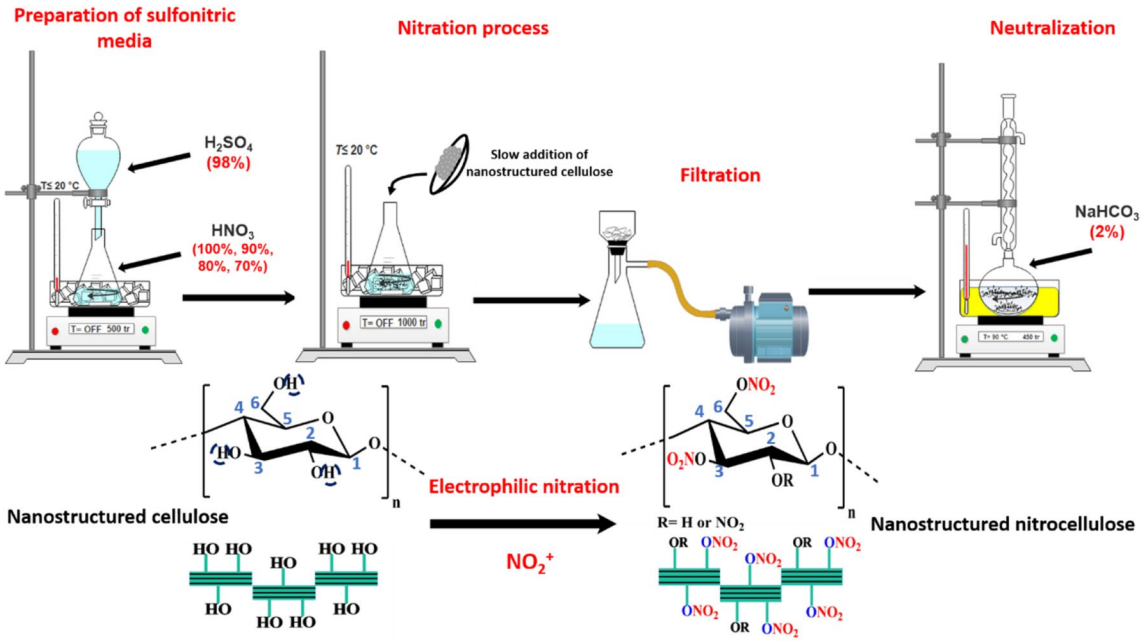

Scheme 1 Nitration pathway for the synthesis of energetic nanostructured cellulosic polymers

researchers have studied the kinetic of cellulose nitration and highlighted that the nitration process is more efficient at the primary OH sites bonded to the C6 carbon compared to the secondary C2 and C3 ones, which display a similar reactivity [9–11].

In general, the nitrating medium used in industrial scale for NC synthesis is composed of a mixture of nitric acid and sulfuric acid, which strongly affects the NO_2^+ content. Given that the formation of this latter is a limiting stage, its concentration can be boosted by increasing the composition of sulfonitric acids, as revealed by many research activities [10, 12, 13]. Therefore, through the selection of mixed acid concentration, cellulose nitrate with various O–NO_2 substitution degree and nitrogen content can be obtained. In addition, it was reported that several parameters of this energetic biopolymer, such as stability, viscosity, hygroscopicity, solubility, and applicability features, depend strongly on the nitrogen content in its molecular structure [14–17]. As an example, at high nitrogen content ($\geq 12\%$), it is classified as an explosive material, and tends to be processed in smokeless gun powders and rocket propellants due to its high flammability and explosiveness [18, 19]. However, NC with low nitrogen content ($\leq 12\%$) can be used as lacquers, inks and as an ingredient in membranes, cosmetic and biomedical products owing to its high mechanical strength and flexibility [20–23].

The inherent characteristics of traditional NC can be further extended through structural modification of its cellulosic precursor to develop promising nanostructured nitrocellulose (NNC) for potential application in high-energy dense formulations. As an important subclass of cellulose nanostructure, cellulose microcrystals, also called microcrystalline cellulose, is a naturally occurring biopolymer conventionally prepared by partial depolymerization of native cellulose using acid hydrolysis to generate highly ordered cellulosic chains with micrometric fiber size [24–28]. According to the literature reports, this type of cellulose derivative displays superior physicochemical and mechanical properties, excellent surface reactivity and interesting thermal stability compared to the ordinary cellulose, which render it highly desirable biopolymer to develop innovative high-value cellulosic materials for widespread uses [29–33]. Recently, the significant achievements in the downscaling technology of cellulosic derivatives have driven the energetic materials community to explore new opportunities to develop the next generation of nitrated nanocellulose with attractive physical stability and energetic performance [34–37]. For instance, it was demonstrated in our previous works that the nitration of structural-modified cellulose instead of pristine cellulose is an efficient approach to obtain an outstanding alternative nitrate ester cellulosic biopolymer with better features than the common NC [38–40]. In addition, due to the destructive capacities of such cellulose-based energetic polymers, a detailed knowledge of their thermal decomposition kinetics could be an excellent complementary approach for establishing and maintaining appropriate safety protocols during their preparation, storage and use, hence facilitating the prevention and mitigation of related accidents [14, 16, 41].

The novelty of the present study is linked to the development of emergent nitrate esters-based nanostructured cellulosic derivatives through sulfonitric esterification of cellulose microcrystals using various nitric acid concentrations. New insights on their physicochemical properties and thermal decomposition kinetics were also provided. In addition, the assessment of the effect of nitric acid concentration can help to optimize the synthesis processes and storage conditions of such hazardous nanostructured materials. Moreover, it may allow providing guidelines for their specific use as promising alternative candidate to replace the conventional NC in high-performance energetic formulations.

Experimental

Materials and chemicals

In this study, the employed starting nanostructured cellulose (Avicel, cellulose microcrystals) was industrial produced by Merck. Concentrated sulfuric acid (H_2SO_4, 98%), fuming nitric acid (HNO_3, 100%) and sodium bicarbonate ($NaHCO_3$) were acquired from VWR-Prolabo. It should be noted that other three concentrations of nitric acid (90%, 80% and 70%) were prepared by a slow addition of 100% nitric acid to the deionized water under magnetic stirring.

Nitration mechanism

The electrophilic nitration of free accessible OH functions of nanostructured cellulose precursor was carried out in water bath ($T \leq 20$ °C) using mixtures of HNO_3/H_2SO_4 (1:2.5, v/v) following the steps depicted in Scheme 1. The ratio of dried precursor over nitric acid and nitration time was fixed at 1:45 (g/ml) and 35 min, respectively, under strong magnetic stirring (1000 rpm). After the nitration process, the mixture was filtered on a vacuum filter and then neutralized under continuous stirring using H_2O heated for 2 h at 90 °C, then $NaHCO_3$ (2%, w/v) solution heated for 2 h at 90 °C, and finally, H_2O heated for 1 h at 90 °C. Subsequently, the stabilized nanostructured nitrocellulose was first dried overnight at room temperature and further at 105 °C for 2 h. All nitration steps were repeated by varying the fuming nitric acid concentration (100%, 90%, 80%, and 70%) to obtain the corresponding white solid NNC-100, NNC-90, NNC-80 and NNC-70. It is important to note that appropriate safety precautions like face shield, leather coat, earthed equipment and kevlar gloves should be taken all the time to avoid any risk of spontaneous ignition during preparing or working with these energetic biopolymers.

Samples characterization

Viscosity assessment

The NNC solutions with different concentrations were prepared by dispersing each synthesized NNC in 0.01 mol/L acetic acid/tetrahydrofuran (THF) solution for 24 h, and filtered by sintered-glass membrane, as described in our previous work [42]. After that, the intrinsic viscosity (η) at infinitely diluted solution (i.e., concentration approaches to zero) of each nitrated sample was determined at 25 °C using an Ubbelohde capillary viscometer with the diameter of 0.55 mm, following the classic method reported in the literature [43, 44]. The viscosity-average molecular weight (M_η) of the investigated NNCs biopolymers was also calculated based on the conventional equation of Mark–Houwink (Eq. 1) for cellulose nitrate esters in THF/0.01 M acetic acid solution [42, 43].

$$[\eta] = 6.44 \times 10^{-2} M_\eta^{0.73} \quad (1)$$

where, η is the intrinsic viscosity (cm^3/g), and M_η is the viscosity-average molecular weight.

Nitrogen content and density

Vario III Elemental analyzer was used to quantify the nitrogen content (Nc) of the designed NNCs polymers. The experiments were performed in triplicate, and the mean value was presented to minimize a rough random error. Their degrees of substitution were then calculated based on the following equation (Eq. 2).

$$\mathrm{DS} = \frac{3.6 \times \text{nitrogen content}(\%)}{31.13 - \text{nitrogen content}(\%)} \quad (2)$$

The experimental densities of the nitrated samples were measured with an electronic Accupyc 1340 II densimeter. Ten analyses, which served to calculate the average density and standard deviation, were done for each individual sample.

Structural analyses and morphology

The chemical structure was analyzed through Fourier-transform infrared spectroscopy (FTIR) by a JASCO FT/IR-4700 type A spectrometer, in the wavenumber range from 4000 to 400 cm^{-1}. All FTIR spectra were recorded in transmittance mode using potassium bromide (KBr) pellets, with an accumulation of 64 scans and a resolution of 4 cm^{-1}.

The crystalline structure was investigated through X-ray diffraction (XRD) measurements using a PANalytical

X'pert PRO Multi-Purpose diffractometer equipped operated at generator settings of 45 kV and 40 mA. The XRD data were collected over an angular range of 5–40°/2θ, a step size 0.017°/2θ and a count time of 50.1650 s per step. The crystallinity index (CrI) of each NNC sample was then calculated according to the Eq. (3) [45].

$$\mathrm{CrI}(\%) = \frac{\sum \mathrm{Scr}}{\sum \mathrm{Scr} + \sum \mathrm{Sam}} \times 100 \tag{3}$$

where *Scr* is the peak area for the crystalline parts, and *Sam* is the peak area for the amorphous domains.

The surface morphologies were examined using a Zeiss model EVO MA scanning electron microscope (SEM) at an operating voltage of 10 kV. To reduce the charging effects, the nitrated samples and their nanostructured cellulosic precursor were coated with gold using a sputter coater.

Thermal behavior

The thermal stability and degradation behavior were investigated using a Perkin-Elmer TGA 4000 and DSC 8000 analyzers. Sample mass of 1–2 mg was placed in a sealed aluminum crucible and heated from 50 to 350 °C at a heating rate of 10 °C/min for TGA analysis, and at various heating rates (5, 10, 15 and 20 °C/min) for DSC experiments. All measurements were recorded under a constant nitrogen atmosphere (30 mL/min) to prevent oxidation effects. Each analysis was performed in triplicates, and the obtained data were found to be highly reproducible.

Isoconversional kinetic analysis

To better understand the thermal runway mechanism of the synthesized nanostructured nitrocellulose biopolymers, their non-isothermal decomposition kinetics were investigated through isoconversional kinetic methods, namely iterative Kissinger–Akahira–Sunose (it-KAS) [46], Trache-Abdelaziz-Siwani (TAS) [47], and non-linear Vyazovkin's method coupled with compensation effect (VYA/CE)) [48]. According to the recommendations of the kinetics committee of the International Confederation for Thermal Analysis and Calorimetry (ICTAC), these model-free approaches provide reliable kinetic parameters, including Arrhenius parameters (activation energy (E_a) and preexponential factor (Log (A)) and the most probable mechanism of decomposition, without requiring any particular reaction model [49, 50]. Broadly, the solid-state reaction kinetics of nitrated cellulose are described by the following basic equation (Eq. 4).

$$\frac{\mathrm{d}\alpha}{\mathrm{d}t} = k(T)f(\alpha) \tag{4}$$

where α refers to the extent of conversion ($0 < \alpha < 1$), $k(T)$ represents the rate constant, and $f(\alpha)$ is the differentiated form of the reaction model. The value of α can be derived from the peak area of the DSC curves, and corresponds to the ratio of the current heat change ΔH at a determined time and temperature to the total reaction heat $\Delta H_{\mathrm{total}}$, as shown in Eq. (5).

$$\alpha = \frac{\int_{t_0}^{t} (\mathrm{d}H/\mathrm{d}t)\mathrm{d}t}{\int_{t_0}^{t_f} (\mathrm{d}H/\mathrm{d}t)\mathrm{d}t} = \frac{\Delta H}{\Delta H_{\mathrm{total}}} \tag{5}$$

In most cases, $k(T)$ is expressed by the Arrhenius equation, and $f(\alpha)$ is substituted by its integral form to obtain the general non-isothermal kinetic equation given below (Eq. 6).

$$g(\alpha) = \int_0^{\alpha} \frac{\mathrm{d}\alpha}{f(\alpha)} = \frac{A}{\beta} \int_{T_0}^{T} \mathrm{e}^{-E_a/RT} \mathrm{d}T \tag{6}$$

where $g(\alpha)$ refers to the integral form of the reaction mechanism, for which several models are reported in the work of Trache et al. [47]. The prediction of the kinetic triplet was conducted by MATLAB software within a conversion range of 0.02 to 0.98 with a step of 0.02. Besides that, it is important to note that the details of the kinetic modeling and calculation procedure using the above mentioned isoconversional methodologies are well explained in our recent works [51–53].

Results and discussion

Physicochemical features

In view of the possible alterations caused by the different used nitric acid concentrations (70%, 80%, 90% and 100%), the nitrogen content, density, intrinsic viscosity and viscosity-average molecular weight of the synthesized nitrate esters biopolymers were evaluated, and the obtained results are given in Table 1.

The foremost finding is that all the evaluated sulfonitric media (HNO_3 (70%)/H_2SO_4 (98%), HNO_3 (80%)/H_2SO_4 (98%), HNO_3 (90%)/H_2SO_4 (98%) and HNO_3 (100%)/H_2SO_4 (98%)) contributed for the synthesis of promising nanostructured nitrocellulose biopolymers with elevated nitration degrees, increased densities and reduced viscosities with respect to those of the traditional NC prepared from various natural sources [42, 43]. Another interesting result is that the increase of HNO_3 concentration causes the raise of nitrogen content from 13.01 for NNC-70 to 13.30 for NNC-100, which is attributed to the increased

Table 1 Physicochemical properties of nitrated nanostructured cellulosic derivatives

Sample	*Nc*(%)	DS	ρ (g/cm^3)	[η] (cm^3/g)	M_η (g/mol)
NNC-70	13.01 ± 0.03	2.58	1.689 ± 0.003	256.54 ± 0.07	85,482
NNC-80	13.15 ± 0.03	2.63	1.696 ± 0.002	298.29 ± 0.08	105,094
NNC-90	13.24 ± 0.03	2.66	1.705 ± 0.003	340.11 ± 0.07	125,787
NNC-100	13.30 ± 0.03	2.69	1.714 ± 0.003	387.37 ± 0.08	150,328
Conventional NC [43]	12.56 ± 0.03	2.44	/	951.42	514,783

amount of NO_2^+, leading to the improvement of the electrophilic diffusion of nitrating species into interior of the polymer framework and the acceleration of the esterification rate [8, 15]. It can be also deduced from Table 1 that the evolution trend of the measured densities and viscosities as a function of HNO_3 content is exactly the same to what is found for the nitrogen content. These findings agreed well with previous studies that reported the relationship between the physicochemical properties of nitrocellulose and its nitration degree [44, 54, 55]. The proportional effect of this latter factor on the density and viscosity parameters of the designed NNCs can be also explained by the higher molecular weight of the incorporated O–NO_2 groups as compared to the OH ones, which in turn leads to an elevation in the hydrodynamic volume of the molecular chains of nitrated glucopyranose units. In addition, it is interesting to point out that the developed NNCs derivatives exhibit awesome densities, which are better than those of some common energetic binders like glycidyl azide polymer (1.29 g/cm^3) [56], poly-glycidyl nitrate (1.4 g/cm^3) [57], poly(3-nitratomethyl-3methyl-oxetane) (1.26 g/cm^3) [58], and comparable to those of recently developed energy-rich cellulosic biopolymers [6, 59]. These outcomes provide evidence for the advantage of using nanostructured cellulose as starting material rather that pristine cellulose to develop new generation of energetic nitrate esters cellulosic derivatives for futuristic defense applications.

Chemical structure and surface morphology

Infrared spectroscopy analysis was performed to examine the molecular structure and the chemical functionalities of the synthesized NNCs and their precursor. Figure 1a shows the comparison between the FTIR spectra of the used nanostructured cellulose and its nitrated derivatives. As can be seen, the starting cellulosic biopolymer displays the typical FTIR profile of a pure cellulose microcrystals with representative chemical groups. The bands recorded at 3335 cm^{-1}, 2903 cm^{-1}, 1430 cm^{-1}, 1160 cm^{-1}, and 891 cm^{-1} related to the stretching vibration of O–H, the C–H symmetrical stretching, the symmetric deformation of CH_2, the C–O–C stretching of the pyranose ring, and the ß-glycosidic linkage vibration, respectively [60–62]. It can be also inferred from Fig. 1a that the most obvious molecular structure alterations that occurred after sulfonitric esterification correspond to the significant decrease in the intensity of OH bands, and the clearly appearance of the characteristic vibrational peaks of nitrate ester moieties. These results prove the effective

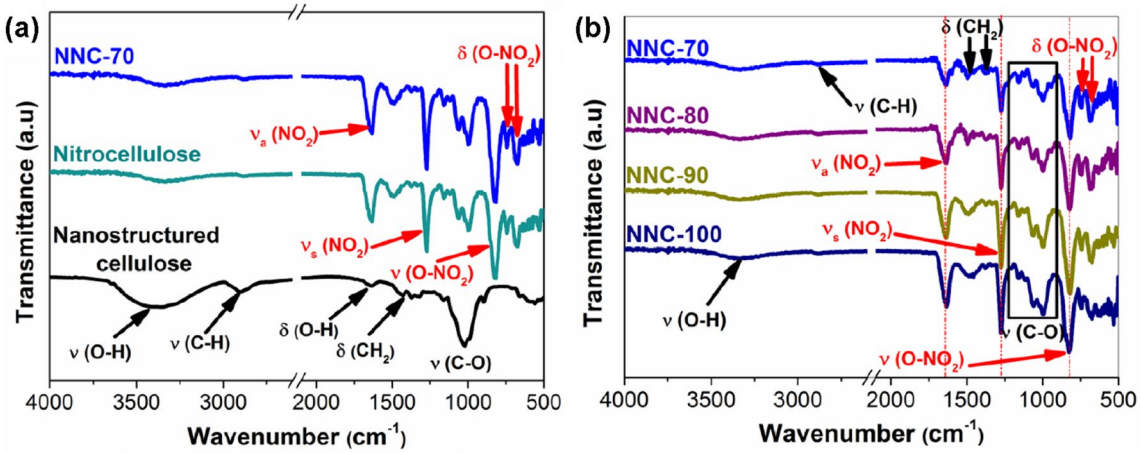

Fig. 1 FTIR spectra of **a** cellulose nanostructure and nitrated cellulosic biopolymers; **b** all nanostructured nitrocelluloses

electrophilic nitration without destruction of the main macromolecule matrix.

On the other hand, the infrared spectra obtained for all the evaluated NNC samples prepared using several HNO_3 concentrations are plotted in Fig. 1a, b. It is perceived that all nitrated derivatives exhibit the well-known vibrational bands of conventional nitrocellulose with slightly higher intensities, which are the stretching and bending vibrations of NO_2 and O–NO_2 functional groups in the right half of spectral domains below 2000 cm^{-1}, demonstrating the successful molecular structure of the produced NNC polymers. This finding also supports the conclusion that the principal nitrocellulose skeleton remains unmodified regardless of nitric acid concentration. It can be also deduced from Fig. 1b that the peak intensities related to the stretching vibrations of the inserted explosophoric groups (NO_2 and O–NO_2) increase while increasing the HNO_3 concentration, which highlights the important effect of HNO_3 content for nitration experiments. This statement can be supported by the measured nitrogen contents and substitution degrees listed in Table 1.

The morphological structure of the nitrated cellulosic biopolymers and their precursors was also examined using SEM to investigate the eventual surface morphology modifications induced by the different performed sulfonitric nitration. As can be observed from Fig. 2, the starting cellulose nanostructure presents a rougher surface and irregular rod-shape structure of aggregated microsized fibrils, also known as microcrystals, with an approximate diameter of 10 µm. Similar surface topography for other commercially available cellulose microcrystals is mentioned elsewhere [30, 54]. The observed bundles of aggregates are due to the strong inter- and intramolecular hydrogen interactions between the elementary microfibrils [63–66]. Besides that, it should be mentioned that the average diameter of elementary microfibers is within the range of 1–10 nm.

After nitration, it can be clearly noticed from Fig. 2 that all the considered sulfonitric media yield NNCs with almost identical surface microstructure as their precursor, demonstrating a homogenous esterification with a uniform distribution of NO_2 groups [7, 34]. Contrary to nanostructured nitrocellulose, conventional cellulose nitrate exhibits long individual fibrous with rough surface instead of clear and smooth ones for its ordinary cellulose precursor, providing evidence for the heterogeneous nitration process already

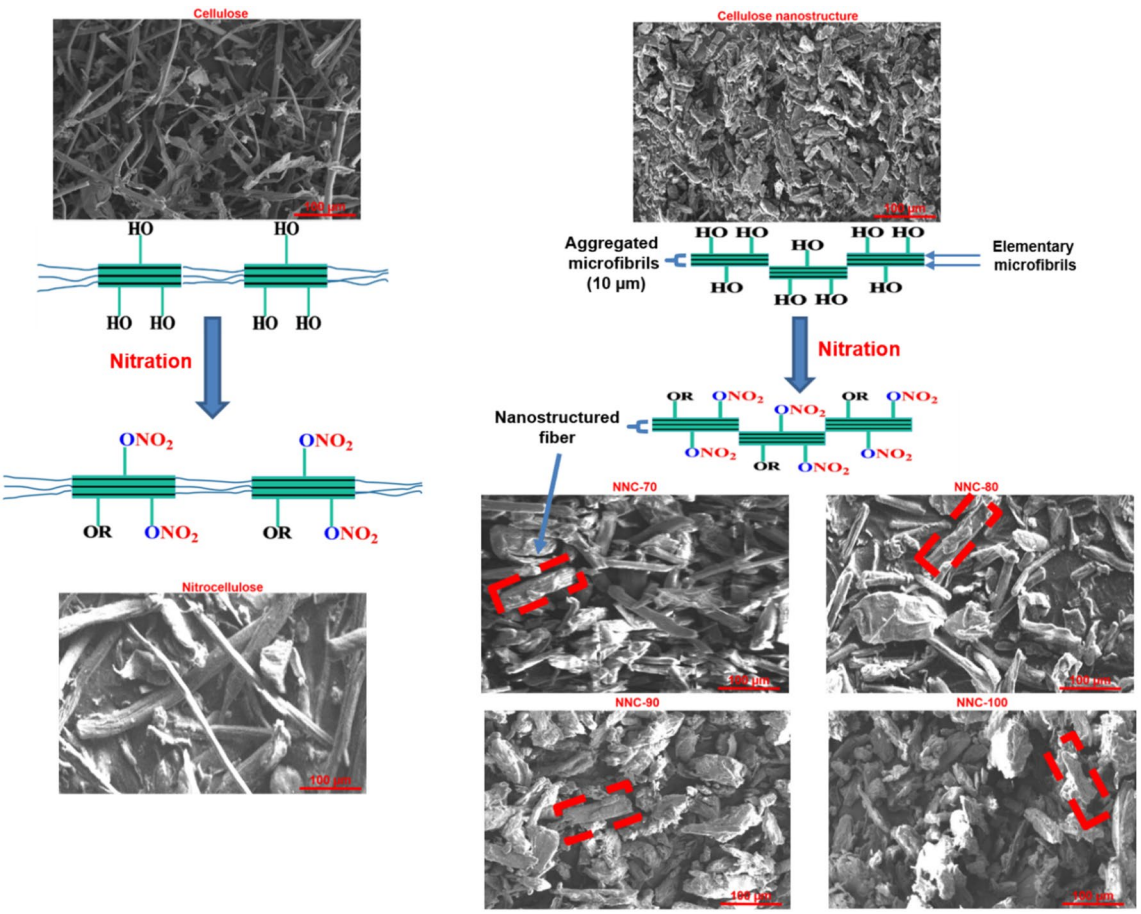

Fig. 2 SEM micrographs of starting cellulosic biopolymers and their nitrated derivatives

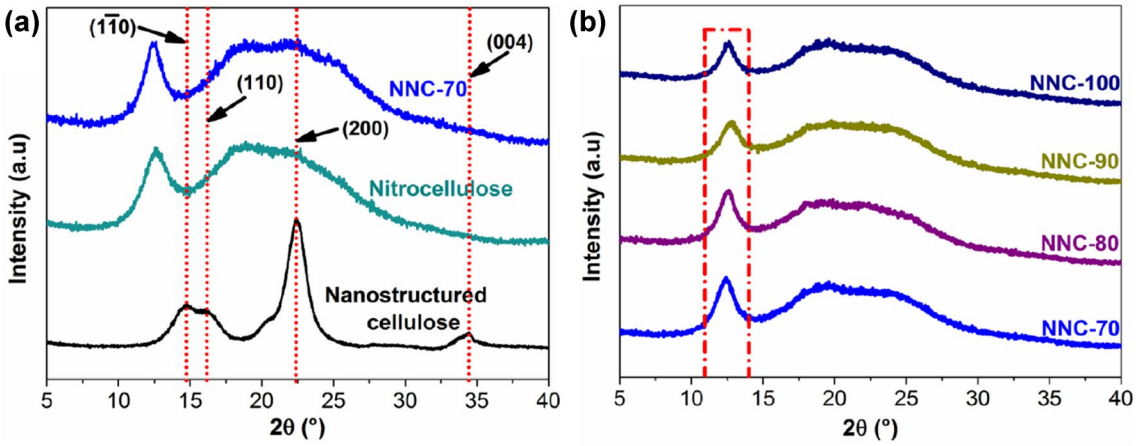

Fig. 3 XRD patterns of **a** cellulose nanostructure and nitrated cellulosic biopolymers; **b** all nanostructured nitrocelluloses

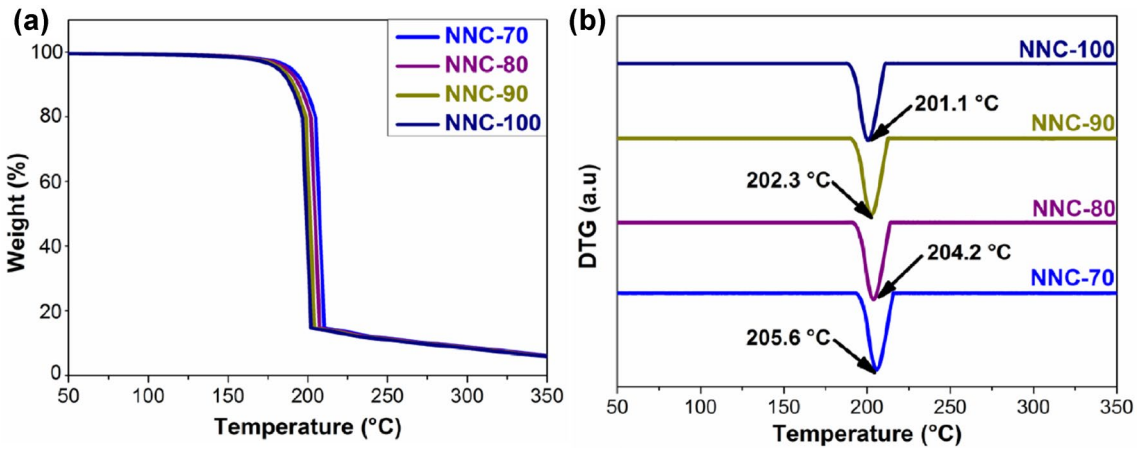

Fig. 4 TGA and DTG thermograms of nitrated nanostructured cellulosic biopolymers at $\beta = 10$ °C/min

mentioned in previous reports [8, 38]. According to the above findings, we can conclude that the type of nitric acid employed in the sulfonitric medium does not alter the morphology of the developed nitrated cellulosic nanostructures. Additionally, it is worth noting that similar reports about the morphological features of structural-modified cellulose and its nitrated derivatives are already highlighted in our previous investigations [10, 29].

Crystallinity features

XRD analyses were conducted to study the crystalline structure of the different nanostructured cellulosic biopolymers, and the obtained patterns illustrated in Fig. 3 are compared. It is clear from Fig. 3a that the starting cellulosic material presents the typical crystallographic planes of cellulose I allomorph observed at 2θ values around 14.8° for (1 $\bar{1}$ 0), 16.5° for (110), 22.4° for (200), and 34.6° for (004) [5, 67]. After nitration, it can be revealed from Fig. 3 that all nitrated samples show similar diffractograms analogous to that of the common nitrocellulose, indicating that the performed esterification reactions using various HNO_3 concentrations have no effect on the main crystalline form of the resulted NNCs. Furthermore, the most detailed changes in the crystalline structure of nitrated derivatives with regard to their cellulosic precursor are the disappearance of the (1 $\bar{1}$ 0), (110) and (004) lattice planes, the broadening of the (200) plane, and the appearance of new diffractions peaks centered at $2\theta = 12.5°$ and 20.1° related to the ordered and amorphous domains of nitrated cellulose chains, respectively [8, 45]. However, it is noticeable from Fig. 3b that the crystalline peak intensity at 12.5° decreases from NNC-70 to NNC-100, suggesting the negative effect of HNO_3 concentration on the crystallinity index.

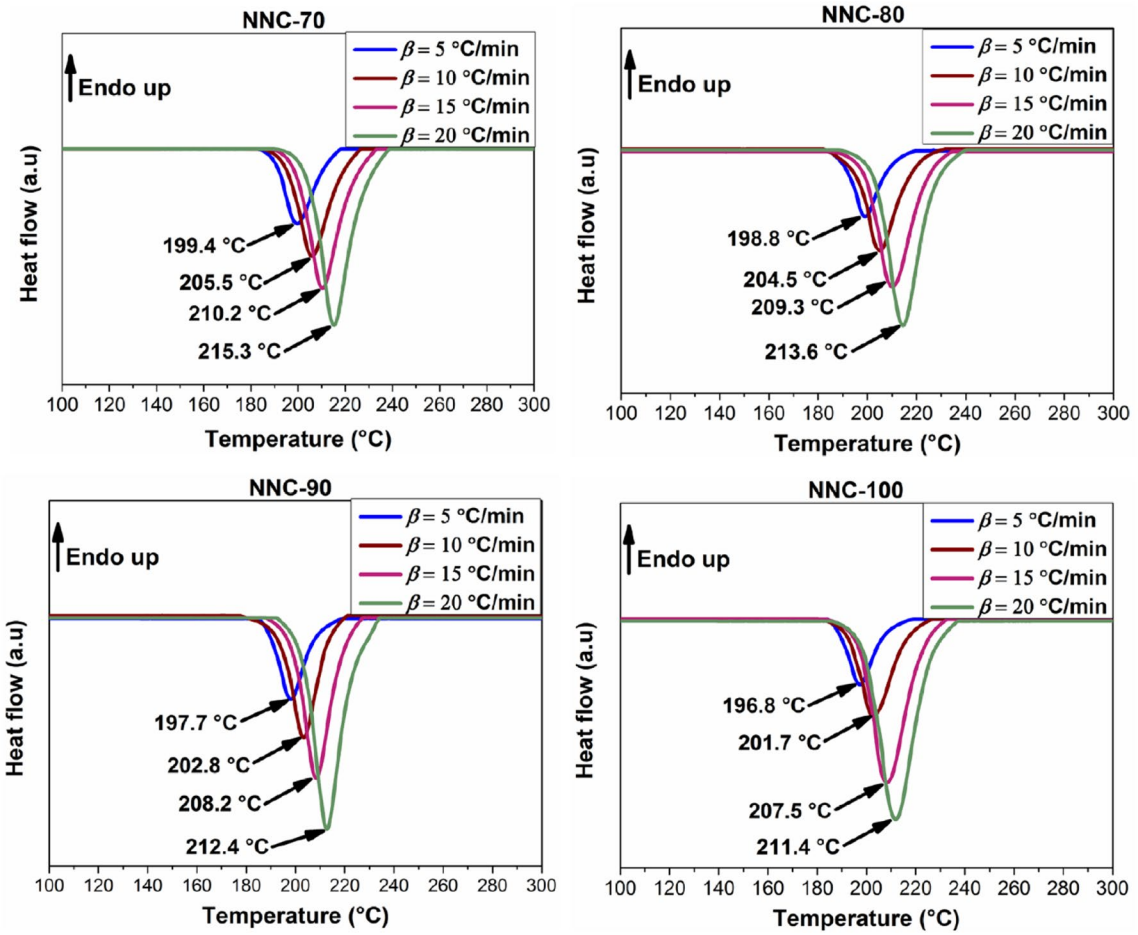

Fig. 5 DSC thermograms of all nitrated nanostructured cellulose polymers at different heating rates

Table 2 DSC data of the synthesized nanostructured cellulose nitrates at various heating rates

Compounds	β (°C/min)	T_{onset} (°C)	T_{peak} (°C)	$/\Delta H/$ (J/g)
NNC-70	5	189.5	199.4	1396.1
	10	194.3	205.5	1555.7
	15	197.7	210.2	1831.5
	20	202.6	215.3	2035.2
NNC-80	5	188.4	198.8	1474.8
	10	192.8	204.5	1662.3
	15	196.7	209.3	1937.5
	20	201.6	213.9	2110.1
NNC-90	5	187.9	197.7	1547.6
	10	191.7	202.8	1756.4
	15	195.3	208.2	2007.8
	20	200.5	212.4	2221.3
NNC-100	5	187.2	196.8	1598.1
	10	190.9	201.7	1803.5
	15	194.8	207.5	2034.9
	20	199.6	211.4	2262.4

To further elucidate the subsequent alteration in crystallinity order caused by the different conducted nitration processes, the crystallinity of all samples was evaluated based on the peak deconvolution of their diffractograms using Pearson VII mathematical function [1, 59]. The calculated *CrI* values are found to be 31.26%, 30.68%, 29.84% and 29.47% for NNC-70, NNC-80, NNC-90 and NNC-100, respectively, which are significantly lower than that of their nanostructured cellulose precursor (78.29%). This expected drop in *CrI* is due to the nitration for which a partial debundling and disintegration of the crystalline phase occurs, followed by the substitution of OH groups with explosophoric O–NO_2 moieties that noticeably reduce the intense hydrogen bonding interactions [6, 43]. Moreover, it is found that the increased HNO_3 concentration lowered the *CrI* of the designed NNC, which is in accordance with nitrogen content evolution, since the growth amount of the incorporated nitrogen-rich O–NO_2 functions with respect to the OH ones entails the increased randomness of the crystalline arrangement. Interestingly, all the developed NNCs reveal greater *CrI* than the common range of the conventional NC

(23–26%), which indicate their superior mechanical properties, and promote their application in high-performance formulations [42, 68, 69].

Thermal properties

Study of the thermal decomposition properties is a crucial criterion in the development of new energetic materials and the judgment of their suitability for real-world applications. Therefore, TGA and DSC analyses were executed to evaluate the thermal stability and degradation behavior of the prepared nanostructured nitrocellulose polymers. It should be noted that the starting nanostructured cellulosic biopolymer displays a single prominent weight loss event associated with an endothermic decomposition peak appeared at onset temperature of 331.7 °C and maximum peak temperature of 348.1 °C for $\beta = 10$ °C/min. This process is assigned to the degradation of polysaccharide framework through the cleavage of glycosidic bonds as discussed in our previous papers [5, 40].

The obtained TGA/DTG thermograms of the developed nanostructured nitrocellulose biopolymers are plotted in Fig. 4. It can be revealed that all NNC samples are characterized by one thermal degradation stage occurred within the temperature range of 180–210 °C, which is corresponded to the main thermolytic cleavage of the linked nitrate esters moieties followed by autocatalytic parallel reactions [35, 52, 70]. Furthermore, it is evident from TGA/DTG curves that the increased concentration of nitric acid from 70 to 100% reduced the thermal decomposition of the resulted energetic NNCs, which is consistent with nitrogen content and crystallinity evolution.

On the other side, the heat flow thermograms of the produced energetic polymers at various heating rates ($\beta = 5$, 10, 15 and 20 °C/min) are plotted in Fig. 5, and the resulted thermal parameters from these curves are given in Table 2. As can be seen, all the investigated NNC samples synthesized using different HNO_3 concentrations present one prominent exothermic decomposition event that occurs at lower temperatures than their nanostructured cellulosic precursor. This finding is attributed to the main thermolysis process caused by the homolytic breaking of the explosophoric and thermally unstable O–NO_2 moieties, leading to the formation of toxic nitrogen oxide species [52, 71, 72]. It is clear that this exothermicity shifted to higher temperatures with

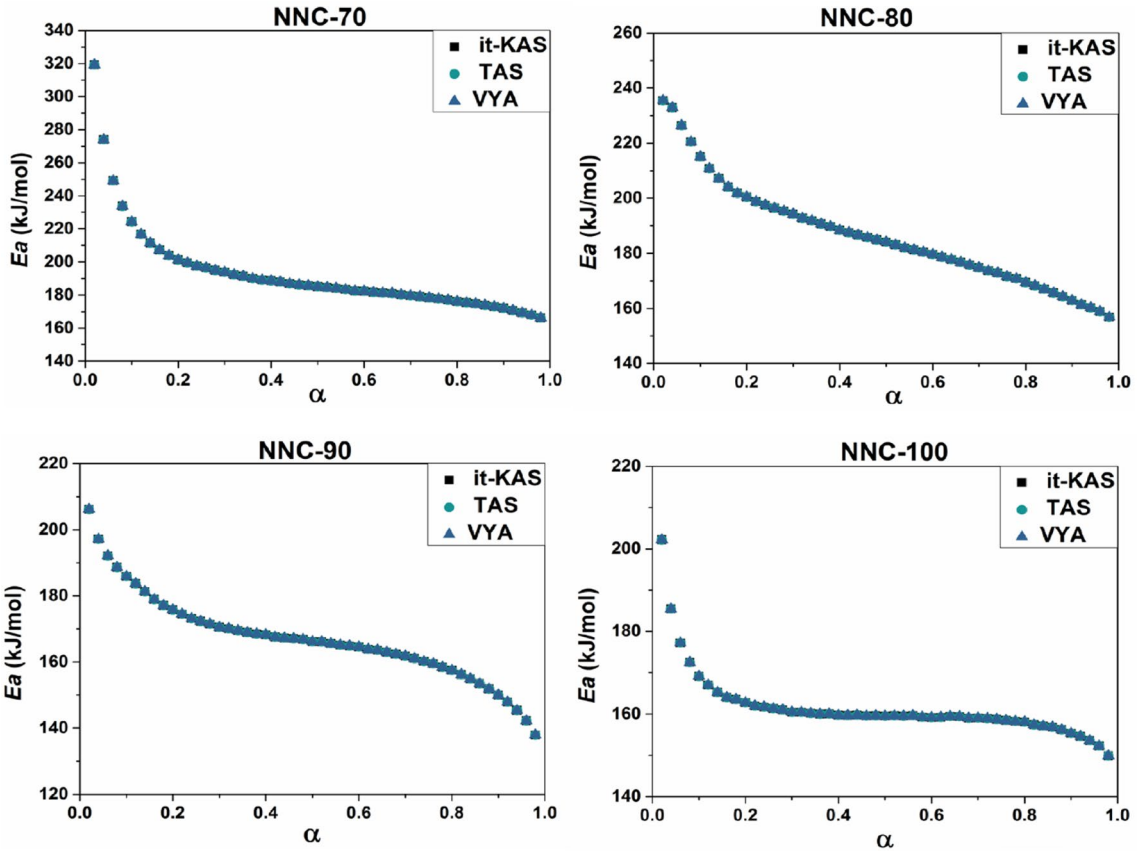

Fig. 6 Activation energy evolution with respect to the extent of conversion for the synthesized nanostructured nitrocelluloses

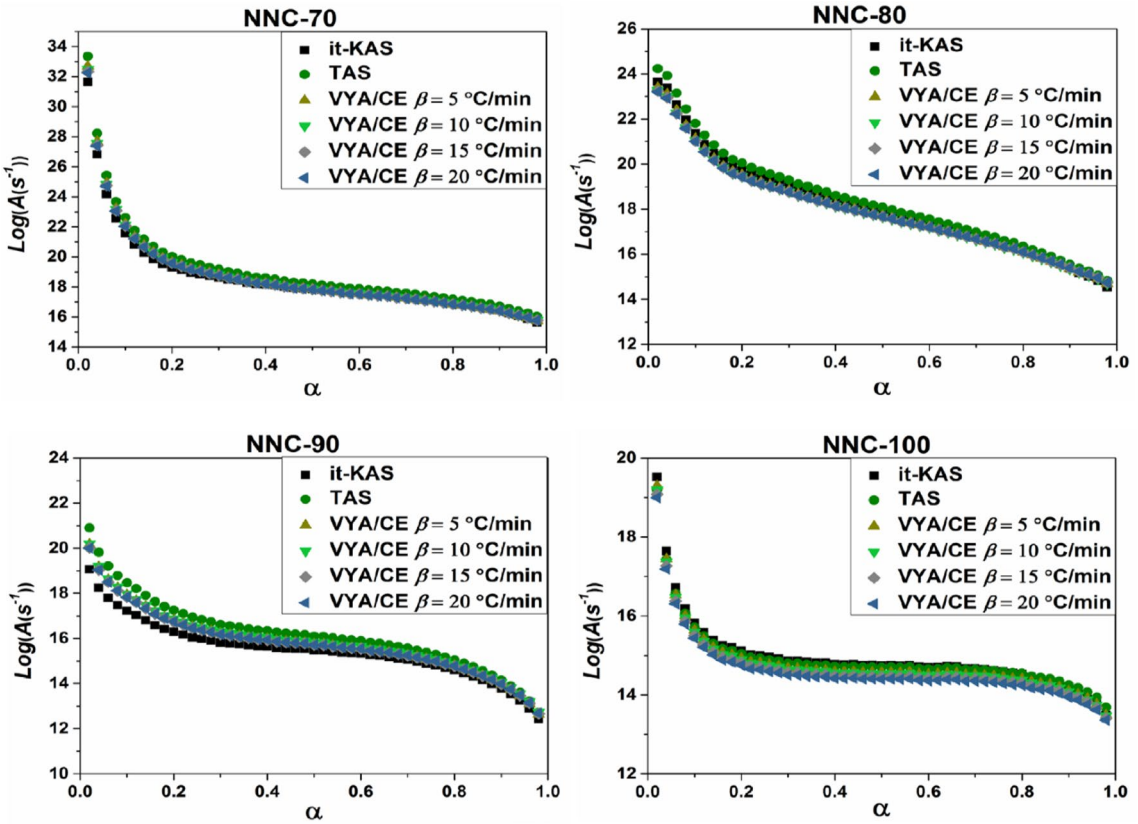

Fig. 7 Evolution of the decimal logarithm of the pre-exponential factor as function of conversion for the synthesized nanostructured nitrocelluloses

the increase of the heating rates due to the fact that the low β provides sufficient time for a regular distribution of temperature around the sample, and thus the pyrolysis starts earlier. At the same β, a slight decline of the pyrolysis temperatures and an increase of the decomposition enthalpy are noticed while increasing the HNO_3 concentration, which is in line with TGA findings. In this context, several researchers have demonstrated that the increased *Nc* as well as the reduced *CrI* could elevate the sample sensitivity against thermal stimuli and improve the volume of released gaseous produced by its combustion [73, 74]. Importantly, the thermal stability of all the designed NNCs is found better than that of recently developed high-energy dense polymers based on cellulose nanostructure, such as carbamated microcrystalline cellulose nitrate (T_{peak} = 186.5 °C, β = 5 °C/min) [11], 2-(1*H*-tetrazol-1-yl)acetate cellulose microcrystals nitrate (T_{peak} = 184.2 °C, β = 5 °C/min) [39], nitrated ethylenediamine-functionalized microcrystalline cellulose (T_{peak} = 184.9 °C, β = 5 °C/min) [59], and other energetic binders reported elsewhere [36, 57].

Kinetic parameters determination

Isoconversional kinetic modeling of the thermal degradation of the evaluated NNCs polymers was carried out based on non-isothermal DSC experiments to determine their kinetic triplet, i.e., the activation energy ($E\alpha$), the frequency factor (Log (A)) and the decomposition mechanism ($g(\alpha)$). It is worthy to mention that, until now, no report is available in the literature regarding the kinetic analysis of nanostructured nitrocellulose biopolymers prepared using various sulfonitric media.

The computational average values of $E\alpha$ and Log (A) with their corresponded uncertainties as well as the most probable integral model of decomposition are depicted in Table 3. It can be revealed that the three computed isoconversional integral methods give close values of Arrhenius parameters for each investigated NNC, demonstrating the accuracy of the performed calculations. The precision of the computed parameters using isoconversional linear approaches (it-KAS and TAS) was also confirmed based on the obtained correlation coefficients R^2 higher than 0.9997. Moreover, the obtained apparent activation energies of all nitrated samples are found to be in good agreement with the pyrolysis

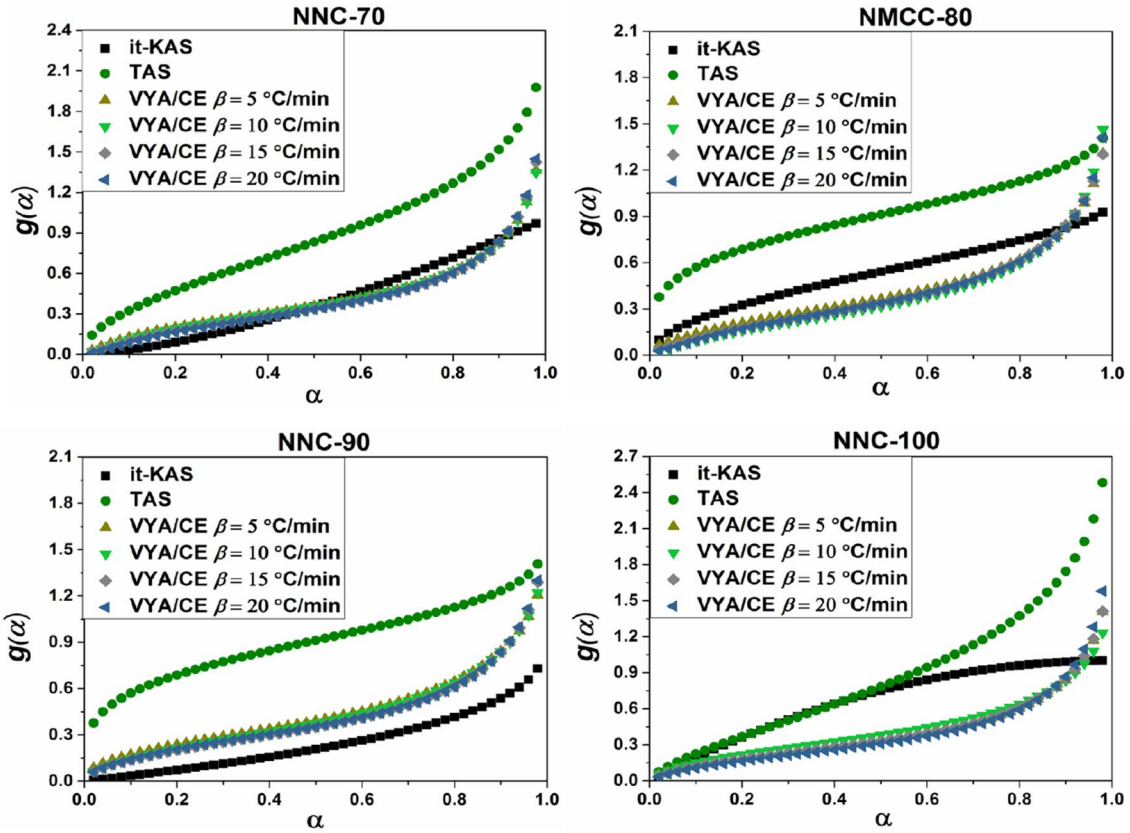

Fig. 8 Evolution of the most probable integral model of decomposition with respect to the extent of conversion for the synthesized nanostructured nitrocelluloses

energy range of nitrated cellulose found in the open literature (150–200 kJ/mol) [30, 75, 76]. Another interesting finding is that the Arrhenius parameters decreased from 193 kJ/mol and 18 s^{-1} for NNC-70 to 161 kJ/mol and 14 s^{-1} for NNC-100. This result can be used as an evidence about the negative impact of nitric acid concentration on the thermal stability of the resulted NNCs and corroborates the findings obtained by TGA and DSC analyses. This evolution trend can be also justified by the effect of nitrogen content in which its increase promotes the beginning of the thermolysis process as shown in previous research activities [16, 74].

The plots of the $E\alpha$ and Log (A) against conversion for all nitrated polymers are illustrated in Figs. 6 and 7, respectively. As can be observed, all the performed model-free approaches (it-KAS, TAS and VYA/CE) provide comparable evolution profiles of Arrhenius parameters for the same nitrate ester material with apparent dependency on the conversion. Furthermore, identical trend of both $E\alpha$ and Log (A) as a function of conversion is perceived, which is explained by the kinetic compensation effect [77]. This relationship between the activation energy and the pre-exponential factor is widely utilized to explain whether the variation on effective $E\alpha$ have physical meaning or they are caused by either the propagation of experimental errors. Besides that, according to Figs. 6 and 7, the Arrhenius parameters of all the synthesized NNCs decrease continuously with the extent of conversion as the decomposition proceeds. Higher values of $E\alpha$ and Log (A) are noted in the beginning of decomposition ($\alpha \leq 0.1$), which are related to the main thermolytic decomposition of energetic O-NO_2 groups and the liberation of reactive products [30, 78]. Next, the two parameters continue their decrease with different rates until reaching their minimal values at the end of the reaction. This behavior is attributed to the autocatalytic parallel reactions caused by the strong oxidizing NO_2 agents and RO· radicals released during the intrinsic decomposition. These latter will promote the heat accumulation and hotspots formation and consequently accelerate the pyrolysis reaction [6, 79–81].

Among the different theoretical forms available in solid-state reactions, the predicted integral models of decomposition $g(\alpha)$ for each involved NNC polymer are plotted in Fig. 8, and their mathematical formulations are included in Table 3. Based on it-KAS approach, NNC-70 decomposes following a power low nucleation mechanism ($P_{3/2}$), NNC-80 shows an unjustified decomposition process (G_7), NNC-90 follows a phase boundary process characterized by a

Table 3 Kinetic parameters obtained by isoconversional integral methods for all nitrated samples

Sample	Isoconversional method		$E\alpha$ (kJ/mol)	Log(A(s^{-1}))	$g(\alpha)$
NNC-70	it-KAS		193.01 ± 8.13	18.67 ± 0.82	$P_{3/2}=\alpha^{3/2}$
	TAS		193.04 ± 8.23	18.98 ± 0.97	$A_{3/2}=[-\ln(1-\alpha)]^{2/3}$
	VYA/CE	β = 5 °C/min	193.02 ± 7.16	18.72 ± 1.62	–
		β = 10 °C/min		18.71 ± 1.49	–
		β = 15 °C/min		18.67 ± 1.44	–
		β = 20 °C/min		18.66 ± 1.44	–
NNC-80	it-KAS		186.34 ± 8.58	18.10 ± 1.35	$G_7=[1-(1-\alpha)^{1/2}]^{1/2}$
	TAS		186.37 ± 9.41	18.26 ± 1.58	$A_{3/2}=[-\ln(1-\alpha)]^{2/3}$
	VYA/CE	β = 5 °C/min	186.35 ± 7.86	17.96 ± 1.29	–
		β = 10 °C/min		17.96 ± 1.19	–
		β = 15 °C/min		17.92 ± 1.19	–
		β = 20 °C/min		17.90 ± 1.19	–
NNC-90	it-KAS		167.05 ± 9.54	15.54 ± 1.24	$R_3=1-(1-\alpha)^{1/3}$
	TAS		167.09 ± 8.87	16.20 ± 1.32	$A_4=[-\ln(1-\alpha)]^{1/4}$
	VYA/CE	β = 5 °C/min	167.06 ± 7.60	15.91 ± 1.16	–
		β = 10 °C/min		15.85 ± 1.16	–
		β = 15 °C/min		15.79 ± 0.98	–
		β = 20 °C/min		15.81 ± 0.98	–
NNC-100	it-KAS		161.46 ± 9.18	14.94 ± 1.11	$A_2=[-\ln(1-\alpha)]^{1/2}$
	TAS		161.49 ± 9.34	14.91 ± 1.39	$A_{2/3}=[-\ln(1-\alpha)]^{3/2}$
	VYA/CE	β = 5 °C/min	161.47 ± 8.45	14.78 ± 0.96	–
		β = 10 °C/min		14.75 ± 0.95	–
		β = 15 °C/min		14.67 ± 0.90	–
		β = 20 °C/min		14.61 ± 0.90	–

deceleratory contracting sphere rate (R_3), while, NNC-100 decomposition is governed by a random nucleation model with a subsequent growth rate (A_2). However, using TAS methodology, it was found that all NNCs exhibit a random Avrami–Erofeev nucleation ($A_{3/2}$, $A_{2/3}$ and A_4), which is considered as an autocatalytic process identified by a sigmoidal decomposition rate for which the rate initially increases with the conversion to reach a maximum, and then decreases at the final stage [49]. Similar kinetic behavior is largely reported for the decomposition mechanism of nitrated cellulose-rich biopolymers [30, 52, 75]. The results herein indicate that different reaction mechanisms could be assigned, which is probably attributed to the different approximations utilized for each isoconversional approach and the nature of the considered compound.

Conclusion

A promising class of energy-rich nanostructured biopolymers was developed through sulfonitric nitration of cellulose microcrystals using various nitric acid concentrations. The experimental findings confirmed that all the evaluated sulfonitric media (HNO_3 (70%)/H_2SO_4 (98%), HNO_3 (80%)/H_2SO_4 (98%), HNO_3 (90%)/H_2SO_4 (98%) and HNO_3 (100%)/H_2SO_4 (98%)) led to the successful formation of the desired nitrate esters cellulosic nanostructures with great nitrogen content and elevated densities compared to the commonly used nitrocellulose. Furthermore, the crystallinity and thermal stability of the as-prepared NNCs were found to decrease with increasing HNO_3 concentration, whereas their nitrogen content, density and viscosity-average molecular weight were promoted from NNC-70 to NNC-100. Additionally, non-isothermal kinetic modeling using isoconversional integral methods (it-KAS, TAS and VYA/CE) revealed a decreased trend of the Arrhenius parameters from NNC-70 to NNC-100 with different decomposition models. These outstanding outcomes will certainly pave the way toward the next generation of nanostructured cellulose-based energetic biopolymers for potential application in composite explosives and advanced high-energy dense formulations.

References

1. Trache, D., Tarchoun, A.F.: Differentiation of stabilized nitrocellulose during artificial aging: Spectroscopy methods coupled with principal component analysis. J. Chemometr. **33**, e3163 (2019)
2. Cherif, M.F., Trache, D., Benaliouche, F., Tarchoun, A.F., Chelouche, S., Mezroua, A.: Organosolv lignins as new stabilizers

for cellulose nitrate: thermal behavior and stability assessment. Int. J. Biol. Macromol. **164**, 794–807 (2020)
3. Sabatini, J.J., Johnson, E.C.: A short review of nitric esters and their role in energetic materials. ACS Omega **6**, 11813–11821 (2021)
4. Yang, M., Kong, Q., Feng, W., Yao, W., Wang, Q.: Caged biomass carbon with anchoring MoO2/NC nanospheres: synergistic enhancement of potassium ion storage and electrochemical performance. Appl. Surf. Sci. **569**, 150984 (2021)
5. Tarchoun, A.F., Trache, D., Klapötke, T.M.: Microcrystalline cellulose from *Posidonia oceanica* brown algae: extraction and characterization. Int. J. Biol. Macromol. **138**, 837–845 (2019)
6. Tarchoun, A.F., Trache, D., Klapötke, T.M., Selmani, A., Saada, M., Chelouche, S., Mezroua, A., Abdelaziz, A.: New insensitive high-energy dense biopolymers from giant reed cellulosic fibers: their synthesis, characterization, and non-isothermal decomposition kinetics. New J. Chem. **45**, 5099–5113 (2021)
7. Liu, J.: Nitrate Esters Chemistry and Technology. Springer, New York (2019).
8. Nikolsky, S.N., Zlenko, D.V., Melnikov, V.P., Stovbun, S.V.: The fibrils untwisting limits the rate of cellulose nitration process. Carbohyd. Polym. **204**, 232–237 (2019)
9. Moniruzzaman, M., Bellerby, J.M., Bohn, M.A.: Activation energies for the decomposition of nitrate ester groups at the anhydroglucopyranose ring positions C2, C3 and C6 of nitrocellulose using the nitration of a dye as probe. Polym. Degrad. Stab. **102**, 49–58 (2014)
10. Sullivan, F., Simon, L., Ioannidis, N., Patel, S., Ophir, Z., Gogos, C., Jaffe, M., Tirmizi, S., Bonnett, P., Abbate, P.: Nitration kinetics of cellulose fibers derived from wood pulp in mixed acids. Ind. Eng. Chem. Res. **57**, 1883–1893 (2018)
11. Tarchoun, A.F., Trache, D., Klapötke, T.M., Krumm, B., Kofen, M.: Synthesis and characterization of new insensitive and high-energy dense cellulosic biopolymers. Fuel **292**, 120347 (2021)
12. Jori Roslan, N., Jamal, S.H., Ong, K.K., Wan Yunus, W.M.Z.: Preliminary study on the effect of sulphuric acid to nitric acid mixture composition, temperature and time on nitrocellulose synthesis based Nata de Coco. In: Solid State Phenomena. Trans Tech Publication, pp. 312–319 (2021)
13. Wang, Q., Gu, Y., Ren, C., Liu, H., Su, P.: Effect of acid concentration on thermal stability of nitrocellulose (NC) for civil use. In: IOP Conference Series: Earth and Environmental Science. IOP Publishing, pp. 022018 (2021)
14. Huang, S., Wei, R., Weng, J., Wang, J.: An experimental study on the effects of ethanol content on the decomposition and burning risks of nitrocellulose. Cellulose **28**, 4595–4609 (2021)
15. Santos, D., Iop, G.D., Bizzi, C.A., Mello, P.A., Mesko, M.F., Balbinot, F.P., Flores, E.M.: A single step ultrasound-assisted nitrocellulose synthesis from microcrystalline cellulose. Ultrasonics Sonochem. **72**, 105453 (2021)
16. Chai, H., Duan, Q., Cao, H., Li, M., Sun, J.: Effects of nitrogen content on pyrolysis behavior of nitrocellulose. Fuel **264**, 116853 (2020)
17. Wang, Z., Dai, L., Yao, J., Guo, T., Hrynsphan, D., Tatsiana, S., Chen, J.: Improvement of *Alcaligenes* sp. TB performance by Fe-Pd/multi-walled carbon nanotubes: enriched denitrification pathways and accelerated electron transport. Bioresour. Technol. **327**, 124785 (2021)
18. Sullivan, F., Simon, L., Ioannidis, N., Patel, S., Ophir, Z., Gogos, C., Jaffe, M., Tirmizi, S., Bonnett, P., Abbate, P.: Chemical reaction modeling of industrial scale nitrocellulose production for military applications. AIChE J. **20**, e16234 (2020)
19. Zhao, N., Ma, H., Yao, E., Yu, Z., An, T., Zhao, F., Yu, X.: Influence of tailored CuO and Al/CuO nanothermites on the thermocatalytic degradation of nitrocellulose and combustion performance of AP/HTPB composite propellant. Cellulose **21**, 1–21 (2021)
20. Tang, R., Alam, N., Li, M., Xie, M., Ni, Y.: Dissolvable sugar barriers to enhance the sensitivity of nitrocellulose membrane lateral flow assay for COVID-19 nucleic acid. Carbohyd. Polym. 118259 (2021).
21. Gismatulina, Y.A., Budaeva, V.V., Sakovich, G.V.: Nitrocellulose synthesis from miscanthus cellulose. Propell. Explos. Pyrot. **43**, 96–100 (2018)
22. Zhang, X., Sun, X., Lv, T., Weng, L., Chi, M., Shi, J., Zhang, S.: Preparation of PI porous fiber membrane for recovering oil-paper insulation structure. J. Mater. Sci. Mater. Electron. **31**, 13344–13351 (2020)
23. Yu, Y., Zhao, Y., Qiao, Y.-L., Feng, Y., Li, W.-L., Fei, W.-D.: Defect engineering of rutile TiO2 ceramics: route to high voltage stability of colossal permittivity. J. Mater. Sci. Technol. **84**, 10–15 (2021)
24. Tarchoun, A.F., Trache, D., Klapötke, T.M., Derradji, M., Bessa, W.: Ecofriendly isolation and characterization of microcrystalline cellulose from giant reed using various acidic media. Cellulose **26**, 7635–7651 (2019)
25. Beroual, M., Boumaza, L., Mehelli, O., Trache, D., Tarchoun, A.F., Khimeche, K.: Physicochemical properties and thermal stability of microcrystalline cellulose isolated from esparto grass using different delignification approaches. J. Polymers Environ. 1–13 (2020).
26. Tarchoun, A.F., Trache, D., Derradji, M., Bessa, W., Belgacemi, R.: Cellulose nanoparticles: extractions. Cellulose Nanoparticles 113–148 (2021).
27. Rajnish, K.N., Samuel, M.S., John, A., Datta, S., Narendhar, C., Balaji, R., Jose, S., Selvarajan, E.: Immobilization of cellulase enzymes on nano and micro-materials for breakdown of cellulose for biofuel production-a narrative review. Int. J. Biol. Macromol. **182**, 1793–1802 (2021)
28. Hu, M., Wang, Y., Yan, Z., Zhao, G., Zhao, Y., Xia, L., Cheng, B., Di, Y., Zhuang, X.: Hierarchical dual-nanonet of polymer nanofibers and supramolecular nanofibrils for air filtration with high filtration efficiency, low air resistance and high moisture permeation. J. Mater Chem. A. **9**, 14093–14100 (2021)
29. Bessa, W., Trache, D., Derradji, M., Bentoumia, B., Tarchoun, A.F., Hemmouche, L.: Effect of silane modified microcrystalline cellulose on the curing kinetics, thermo-mechanical properties and thermal degradation of benzoxazine resin. Int. J. Biol. Macromol. **180**, 194–202 (2021)
30. Tarchoun, A.F., Trache, D., Klapötke, T.M., Belmerabet, M., Abdelaziz, A., Derradji, M., Belgacemi, R.: Synthesis, characterization, and thermal decomposition kinetics of nitrogen-rich energetic biopolymers from aminated giant reed cellulosic fibers. Ind. Eng. Chem. Res. (2020).
31. Kian, L.K., Saba, N., Jawaid, M., Fouad, H.: Characterization of microcrystalline cellulose extracted from olive fiber. Int. J. Biol. Macromol. (2020).
32. Rani, A., Reddy, R., Sharma, U., Mukherjee, P., Mishra, P., Kuila, A., Sim, L.C., Saravanan, P.: A review on the progress of nanostructure materials for energy harnessing and environmental remediation. J. Nanostruct. Chem. **8**, 255–291 (2018)
33. Zhang, K., Qiu, L., Tao, J., Zhong, X., Lin, Z., Wang, R., Liu, Z.: Recovery of gallium from leach solutions of zinc refinery residues by stepwise solvent extraction with N235 and Cyanex 272. Hydrometallurgy **205**, 105722 (2021).
34. Dobrynin, O.S., Zharkov, M.N., Kuchurov, I.V., Fomenkov, I.V., Zlotin, S.G., Monogarov, K.A., Meerov, D.B., Pivkina, A.N., Muravyev, N.V.: Supercritical antisolvent processing of nitrocellulose: downscaling to nanosize, reducing friction sensitivity and introducing burning rate catalyst. Nanomaterials **9**, 1386 (2019)

35. Okada, K., Saito, Y., Akiyoshi, M., Endo, T., Matsunaga, T.: Preparation and characterization of nitrocellulose nanofiber. Propell. Explos. Pyrot. **46**, 1–8 (2021)
36. Meng, X., Pu, C., Cui, P., Xiao, Z.: Preparation, thermal and sensitivity properties of nano-sized spherical nitrocellulose composite crystal. Propell. Explos. Pyrot. **45** (2020).
37. Tarchoun, A.F., Trache, D., Klapötke, T.M., Khimeche, K.: Tetrazole-functionalized microcrystalline cellulose: a promising biopolymer for advanced energetic materials. Chem. Eng. J. **400**, 125960 (2020)
38. Tarchoun, A.F., Trache, D., Klapötke, T.M., Krumm, B., Mezroua, A., Derradji, M., Bessa, W.: Design and characterization of new advanced energetic biopolymers based on surface functionalized cellulosic materials. Cellulose 1–17 (2021).
39. Tarchoun, A.F., Trache, D., Klapötke, T.M., Abdelaziz, A., Derradji, M., Bekhouche, S.: Chemical design and characterization of cellulosic derivatives containing high-nitrogen functional groups: towards the next generation of energetic biopolymers. Defence Technol. (2021).
40. Tarchoun, A.F., Trache, D., Klapötke, T.M., Krumm, B., Khimeche, K., Mezroua, A.: A promising energetic biopolymer based on azide-functionalized microcrystalline cellulose: synthesis and characterization. Carbohyd. Polym. 116820 (2020).
41. Gao, X., Jiang, L., Xu, Q., Wu, W.-Q., Mensah, R.A.: Thermal kinetics and reactive mechanism of cellulose nitrate decomposition by traditional multi kinetics and modeling calculation under isothermal and non-isothermal conditions. Ind. Crops Prod. **145**, 112085 (2020)
42. Tarchoun, A.F., Trache, D., Klapötke, T.M., Chelouche, S., Derradji, M., Bessa, W., Mezroua, A.: A promising energetic polymer from *Posidonia oceanica* brown algae: synthesis, characterization, and kinetic modeling. Macromol. Chem. Phys. **220**, 1900358 (2019)
43. Trache, D., Khimeche, K., Mezroua, A., Benziane, M.: Physicochemical properties of microcrystalline nitrocellulose from Alfa grass fibres and its thermal stability. J. Therm. Anal. Calorim. **124**, 1485–1496 (2016)
44. Luo, Q., Zhu, J., Li, Z., Duan, X., Pei, C., Mao, C.: The solution characteristics of nitrated bacterial cellulose in acetone. New J. Chem. **42**, 18252–18258 (2018)
45. Trache, D., Tarchoun, A.F., Chelouche, S., Khimeche, K.: New insights on the compatibility of nitrocellulose with aniline-based compounds. Propell. Explos. Pyrot. **44**, 970–979 (2019)
46. Trache, D., Maggi, F., Palmucci, I., DeLuca, L.T.: Thermal behavior and decomposition kinetics of composite solid propellants in the presence of amide burning rate suppressants. J. Therm. Anal. Calorim. **132**, 1601–1615 (2018)
47. Trache, D., Abdelaziz, A., Siouani, B.: A simple and linear isoconversional method to determine the pre-exponential factors and the mathematical reaction mechanism functions. J. Therm. Anal. Calorim. **128**, 335–348 (2017)
48. Sbirrazzuoli, N.: Determination of pre-exponential factor and reaction mechanism in a model-free way. Thermochim. Acta 178707 (2020).
49. Vyazovkin, S., Burnham, A.K., Favergeon, L., Koga, N., Moukhina, E., Pérez-Maqueda, L.A., Sbirrazzuoli, N.: ICTAC Kinetics Committee recommendations for analysis of multi-step kinetics. Thermochim. Acta 178597 (2020).
50. Granado, L., Sbirrazzuoli, N.: Isoconversional computations for nonisothermal kinetic predictions. Thermochim. Acta **697**, 178859 (2021)
51. Chelouche, S., Trache, D., Tarchoun, A.F., Abdelaziz, A., Khimeche, K., Mezroua, A.: Organic eutectic mixture as efficient stabilizer for nitrocellulose: kinetic modeling and stability assessment. Thermochim. Acta **673**, 78–91 (2019)
52. Benhammada, A., Trache, D., Kesraoui, M., Tarchoun, A.F., Chelouche, S., Mezroua, A.: Synthesis and characterization of α-Fe2O3 nanoparticles from different precursors and their catalytic effect on the thermal decomposition of nitrocellulose. Thermochim. Acta 178570 (2020).
53. Hanafi, S., Trache, D., He, W., Xie, W.-X., Mezroua, A., Yan, Q.-L.: Catalytic effect of 2D-layered energetic hybrid crystals on the thermal decomposition of 3-nitro-2, 4-dihydro-3H-1, 2, 4-triazol-5-one (NTO). Thermochim. Acta **692**, 178747 (2020)
54. He, Y., He, Y., Liu, J., Li, P., Chen, M., Wei, R., Wang, J.: Experimental study on the thermal decomposition and combustion characteristics of nitrocellulose with different alcohol humectants. J. Hazard Mater **340**, 202–212 (2017)
55. de la Ossa, M.Á.F., López-López, M., Torre, M., García-Ruiz, C.: Analytical techniques in the study of highly-nitrated nitrocellulose. TrAC Trends Anal. Chem. **30**, 1740–1755 (2011)
56. Paraskos, A.J.: Energetic polymers: synthesis and applications. Energetic materials, pp. 91–134. Springer, New York (2017)
57. Betzler, F.M., Hartdegen, V.A., Klapötke, T.M., Sproll, S.M.: A new energetic binder: glycidyl nitramine polymer. Cent. Eur. J. Energ. Mater. **13** (2016).
58. Badgujar, D., Talawar, M., Zarko, V., Mahulikar, P.: New directions in the area of modern energetic polymers: an overview. Combus. Explos. Shock Waves **53**, 371–387 (2017)
59. Tarchoun, A.F., Trache, D., Klapötke, T.M., Krumm, B.: New insensitive nitrogen-rich energetic polymers based on amino-functionalized cellulose and microcrystalline cellulose: synthesis and characterization. Fuel **277**, 118258 (2020)
60. Beroual, M., Trache, D., Mehelli, O., Boumaza, L., Tarchoun, A.F., Derradji, M., Khimeche, K.: Effect of the delignification process on the physicochemical properties and thermal stability of microcrystalline cellulose extracted from date palm fronds. Waste Biomass Valori 1–15 (2020).
61. Hachaichi, A., Kouini, B., Kian, L.K., Asim, M., Jawaid, M.: Extraction and characterization of microcrystalline cellulose from date palm fibers using successive chemical treatments. J. Polymers Environ. 1–10 (2021).
62. Meftahi, A., Khajavi, R., Rashidi, A., Rahimi, M., Bahador, A.: Preventing the collapse of 3D bacterial cellulose network via citric acid. J. Nanostruct. Chem. **8**, 311–320 (2018)
63. Hu, L.-B., Huang, X.-Y., Zhang, S., Chen, X., Dong, X.-H., Jin, H., Jiang, Z.-Y., Gong, X.-R., Xie, Y.-X., Li, C.: MoO3 structures transition from nanoflowers to nanorods and their sensing performances. (2021).
64. Mokhena, T.C., Sadiku, E.R., Mochane, M.J., Ray, S.S., John, M.J., Mtibe, A.: Mechanical properties of cellulose nanofibril papers and their bionanocomposites: a review. Carbohyd. Polym. 118507 (2021).
65. Wu, H., Zhang, F., Zhang, Z.: Droplet breakup and coalescence of an internal-mixing twin-fluid spray. Phys. Fluids **33**, 013317 (2021)
66. Wang, X., Li, C., Zhang, Y., Said, Z., Debnath, S., Sharma, S., Yang, M., Gao, T.: Influence of texture shape and arrangement on nanofluid minimum quantity lubrication turning. Int. J. Adv. Manuf. Technol. 1–16 (2021).
67. Benhamou, A.A., Kassab, Z., Nadifiyine, M., Salim, M.H., Sehaqui, H., Moubarik, A., El Achaby, M.: Extraction, characterization and chemical functionalization of phosphorylated cellulose derivatives from giant reed plant. Cellulose 1–18 (2021).
68. Fu, Y., Chen, H., Guo, R., Huang, Y., Toroghinejad, M.R.: Extraordinary strength-ductility in gradient amorphous structured Zr-based alloy. J. Alloys Compds. **888**, 161507 (2021).
69. Zhang, X., Tang, Y., Zhang, F., Lee, C.S.: A novel aluminum–graphite dual-ion battery. Adv. Energy Mater. **6**, 1502588 (2016)

70. Huo, J., Fu, L., Zhao, C., He, C.: Hydrogen generation of ammonia borane hydrolysis catalyzed by Fe22@ Co58 core-shell structure. Chinese Chem. Lett. (2021).
71. Trache, D., Tarchoun, A.F.: Stabilizers for nitrate ester-based energetic materials and their mechanism of action: a state-of-the-art review. J. Mater. Sci. **53**, 100–123 (2018)
72. Sun, R., He, C., Fu, L., Huo, J., Zhao, C., Li, X., Song, Y., Wang, S.: Defect engineering for high-selection-performance of NO reduction to NH3 over CeO2 (111) surface: a DFT study. Chinese Chem. Lett. (2021).
73. He, C., Wang, H., Fu, L., Huo, J., Zheng, Z., Zhao, C., An, M.: Principles for designing CO2 adsorption catalyst: Serving thermal conductivity as the determinant for reactivity. Chinese Chem. Lett. (2021).
74. Cieślak, K., Gańczyk-Specjalska, K., Drożdżewska-Szymańska, K., Uszyński, M.: Effect of stabilizers and nitrogen content on thermal properties of nitrocellulose granules. J. Therm. Anal. Calorim. 1–12 (2020).
75. Cherif, M.F., Trache, D., Benaliouche, F., Chelouche, S., Tarchoun, A.F., Mezroua, A.: Effect of Kraft lignins on the stability and thermal decomposition kinetics of nitrocellulose. Thermochim. Acta **692**, 178732 (2020)
76. Zhao, Y., Jin, B., Peng, R., Ding, L., Zheng, T.: Novel fullerene-based stabilizer for scavenging nitroxide radicals and its behavior during thermal decomposition of nitrocellulose. J. Hazard Mater. **391**, 121857 (2020)
77. Mianowski, A., Radko, T., Siudyga, T.: Kinetic compensation effect of isoconversional methods. React. Kinet. Mech. Catal. **132**, 37–58 (2021)
78. Wu, H., Zhang, F., Zhang, Z.: Fundamental spray characteristics of air-assisted injection system using aviation kerosene. Fuel **286**, 119420 (2021)
79. He, C., Wang, J., Fu, L., Zhao, C., Huo, J.: Associative vs. dissociative mechanism: electrocatalysis of nitric oxide to ammonia. Chinese Chem. Lett. (2021).
80. Li, Y., Macdonald, D.D., Yang, J., Qiu, J., Wang, S.: Point defect model for the corrosion of steels in supercritical water: Part I, film growth kinetics. Corros. Sci. **163**, 108280 (2020)
81. Wang, R., Xie, H., Lai, X., Liu, J.-B., Li, J., Qiu, G.: Visible light-enabled iron-catalyzed selenocyclization of *N*-methoxy-2-alkynylbenzamide. Mol. Catal. **515**, 111881 (2021)